Spin dynamics in the unconventional multiferroic AgCrS$_2$

F. Damay,[1,*] S. Petit,[1] M. Braendlein,[1] S. Rols,[2] J. Ollivier,[2] C. Martin,[3] and A. Maignan[3]

[1]*Laboratoire Léon Brillouin, CEA-CNRS UMR 12, 91191 GIF-SUR-YVETTE CEDEX, France*
[2]*Institut Laue-Langevin, 6 rue Jules Horowitz, Boîte Postale 156, 38042 GRENOBLE CEDEX 9, France*
[3]*Laboratoire CRISMAT, CNRS UMR 6508, 6 Boulevard Maréchal Juin, 14050 CAEN CEDEX, France*

The magnetic excitation spectrum of AgCrS$_2$, a layered multiferroic compound with a collinear four-sublattice antiferromagnetic order, has been investigated by means of time-of-flight inelastic neutron scattering between 5 and 300 K. Coupling mean-field and spin-wave calculations, the experimental spectrum is well reproduced introducing, in the model Hamiltonian, a ferromagnetic exchange interaction between nearest neighbors and a non-negligible antiferromagnetic in-plane next-nearest-neighbor interaction. This study shows that the sign of the magnetic interaction between chromium ions depends on the Cr-Cr distance with a threshold value above which it becomes ferromagnetic and emphasizes the role of the magnetoelastic coupling in the understanding of the physical properties of AgCrS$_2$.

I. INTRODUCTION

Multiferroic materials, in which two or all three ferroic-order parameters [ferroelectricity, (antiferro)magnetism, and ferroelasticity] are observed, have been the subject of intensive research in recent years. Such systems are rather rare in nature but are potentially interesting for a wide range of technological applications.[1,2] In the "spin-driven ferroelectrics," it is the noncollinear spin spiral structure which is responsible for the inversion symmetry breaking,[3,4] which results in a spontaneous polarization below the magnetic-ordering temperature. Frustrated magnets, which often exhibit noncollinear magnetic structures, have, as a result, been investigated extensively, with a special mention to the family of stacked triangular lattices, whose most-known examples are the delafossite CuFeO$_2$ (Refs. 5 and 6) and ACrO$_2$ compounds [A = Cu,[7,8] Ag,[9] Li, and Na (Refs. 9–11)]. In centrosymmetric CuCrO$_2$, for instance, the transition to the noncollinear magnetic state[7,12] coincides with a spontaneous ferroelectric polarization, which reaches 30 μC m^{-2} at 5 K.[9] Pure CuFeO$_2$ has, in contrast, a collinear magnetic ground state of the four-sublattice type [(4SL) or ↑↑↓↓],[5,13] which precludes multiferroic properties, in agreement with the spin-driven theoretical models.[14,15]

Recently, spontaneous polarization was evidenced in AgCrS$_2$,[16] a compound with a stacked triangular topology, structurally closely related to the delafossite family. In AgCrS$_2$, spins order *collinearly* at T_N = 40.5 K, to form a stacking of double ferromagnetic stripes arranged antiferromagnetically, akin to a 4SL-type structure.[17] This magnetic transition actually comes along with a first-order structural transition, which involves a symmetry lowering from the polar $R3m$ structure[18–20] [Fig. 1(a)] towards the ferroelectric monoclinic phase: The Cr triangular lattice undergoes an "isosceles-type" distortion, each triangle having one long and two short Cr-Cr bonds,[17] a fact pointing out the role of the lattice degree of freedom in stabilizing the 4SL magnetic structure.[21] In this context, the matters that naturally arise are the understanding of the impact of the crystal distortion on the magnetic exchange paths and, consequently, on the magnetic ground state, and whether ferroelectricity derives solely from large atomic displacements at T_N or not.

To shed light on these issues, inelastic-neutron-scattering [time-of-flight (TOF)] measurements were performed on polycrystalline AgCrS$_2$ between 5 and 300 K in order to get the dynamical structure factor $S(Q,\omega)$ and its temperature evolution. Mean-field and spin-wave calculations were performed subsequently to find a reliable set of magnetic exchange parameters reproducing the experimental excitation spectrum. Results confirm that the monoclinic distortion of the triangular lattice has a major impact on the nearest-neighbor magnetic exchange, which becomes ferromagnetic along the longest Cr-Cr bond but remains weakly antiferromagnetic along the two shortest ones. Antiferromagnetic next-nearest-neighbor interaction still remains crucial for stabilizing the 4SL phase, a result that underlines, such as in CuCrO$_2$ and CuFeO$_2$, the importance of that kind of exchange in the understanding of the magnetic properties of triangular lattices.

II. EXPERIMENT

Five grams of polycrystalline AgCrS$_2$ were prepared by high-temperature solid-state reaction. Powders of Ag, Cr, and S precursors were weighted according to the stoichiometric ratio. The resulting powder was carefully ground, was pressed in the shape of bars, and was heated in an evacuated silica tube at 900 °C for 12 h. The sample was then checked by room-temperature x-ray diffraction and was found to be single phase. This sample was used for the earlier study[17] mentioned in the Introduction.

TOF inelastic-neutron-scattering experiments were performed using the thermal spectrometer IN4 at the Institut Laue-Langevin [(ILL), Grenoble] with various incident wavelength settings (λ_i = 1.1, 1.6, and 3.2 Å). At 1.6 Å, the instrumental resolution is ~0.7 meV. Additional inelastic TOF data were taken on the IN5 (ILL) cold neutron spectrometer (λ_i = 5.0 Å) with a higher resolution of 80 μeV.

III. RESULTS AND DISCUSSION

A. A. Inelastic scattering results

Figure 2(a) shows the temperature evolution of the powder averaged $S(Q,\omega)$ maps of AgCrS$_2$, recorded on IN4 with an
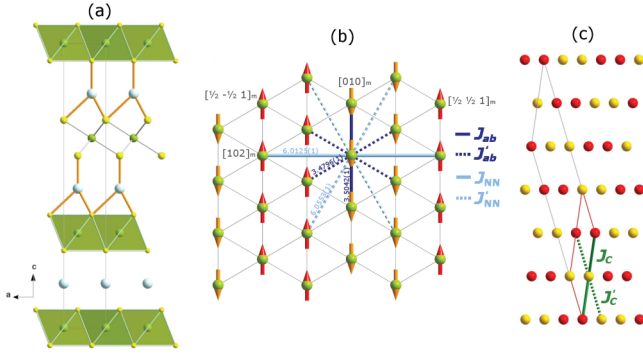
FIG. 1. (Color online) (a) Layered structure of AgCrS$_2$ ($R3m$ space group). Compact layers of CrO$_6$ octahedra are shown in green (gray). In (b) and (c) are illustrated the projections within the triangular plane and along b_m, respectively, of the four-sublattice magnetic structure of AgCrS$_2$. Distances at 10 K (from Ref. [17]) are in angstroms in (b). In (c), the monoclinic Cm cell is outlined in red (dark gray), the (0 0 0.25) magnetic cell is in thin light gray. The different exchange paths J_{ab}, J_{NN}, and J_C are indicated by full colored lines (dark blue (dark gray), light blue (light gray), and green [thick gray lines in (c)], respectively, the degenerate exchange paths J'_{ab}, J'_{NN}, and J'_C, along which the ↑↑↓↓ configuration is found, are indicated by dotted colored lines with the same color scheme.

incident wavelength of $\lambda = 1.6$ Å. Above T_N, from 70 to 42 K, a broad magnetic scattering signal is observed at low Q. As can be better visualized on the 70-K map recorded at $\lambda = 3.2$ Å [Fig. 3(a)] and on the corresponding $\omega = 1$-meV profile [Fig. 3(b)], the Q dependence of this signal does not follow the form factor of the Cr^{3+} ion as would be expected in the case of paramagnetic Cr^{3+} but, instead, shows a correlation peak around 0.6 Å^{-1}. The constant $Q = 0.6$ Å^{-1} profile of this signal exhibits the usual Lorentzian shape of a quasielastic-like scattering with a FWHM of 1.7(3) meV [Fig. 3(c)]. This characterizes slow magnetic fluctuations corresponding to a Cr-Cr distance of about 6 to 7 Å,[17] thus, involving next-nearest-neighbor interactions, which persist well above T_N, a behavior often observed in layered compounds.[8] Broad diffuse scattering centered around 1.9 Å^{-1} is also observed.

As the temperature is lowered below T_N, there is a redistribution of the magnetic intensity, and two new features become visible, a signal around 17 meV extending up to 3 Å^{-1} and a signal around 8 meV centered around 2 Å^{-1} as shown in Fig. 2(b). Below 40.5 K, AgCrS$_2$ exhibits long-range antiferromagnetic order,[17] and these features are, therefore, attributed to the spin-wave dispersion associated with the magnetic ordering. In this picture, the 17-meV feature can be seen as the top of the excitation band [a low-temperature spectrum measured at $\lambda = 1.1$ Å (not shown) confirms that there is no additional excitation, up to 62 meV]. To access the part of the dispersion emerging from the low-Q magnetic Bragg peaks (at $Q = 0.65$ and 0.75 Å^{-1}), large incident wavelength measurements using the IN5 spectrometer (experimental resolution $\delta E = 0.08$ meV) were performed, which actually evidence an easy-axis-like anisotropy gap at $Q = 0.65$ and 0.75 Å^{-1} [Fig. 4(a)]. The value of this gap can be estimated to be about 0.7 meV [Fig. 4(b)] as is further supported by the absence of any excitation in the Q scan at
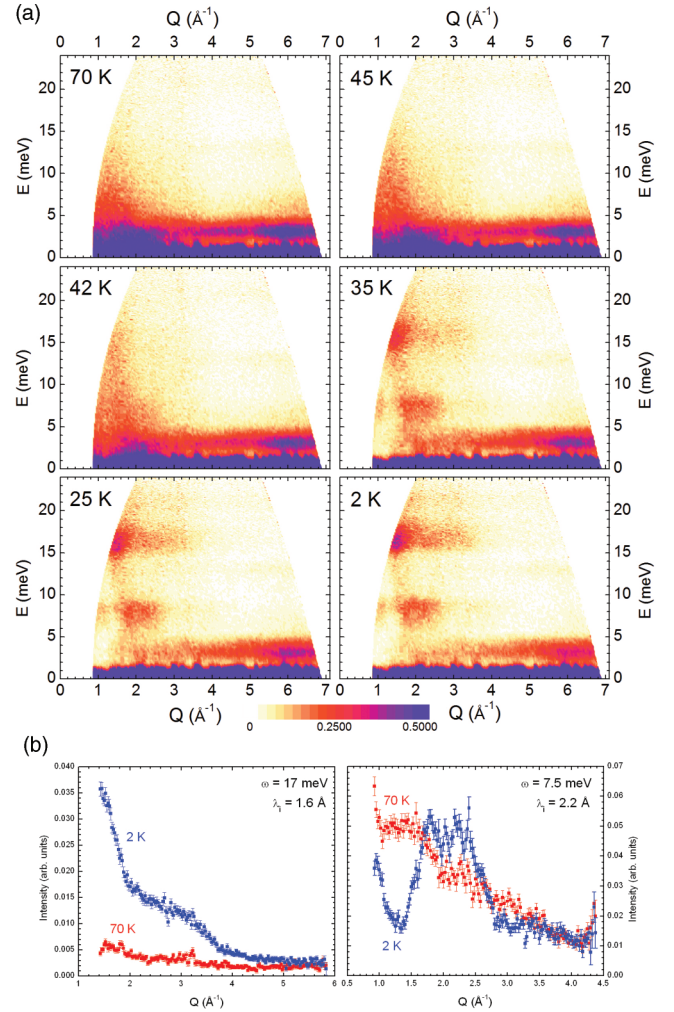
FIG. 2. (Color online) (a) Temperature evolution of the dynamical structure factor $S(Q,\omega)$ (IN4 data, $\lambda = 1.6$ Å) of polycrystalline AgCrS$_2$. (b) Constant energy transfer profiles at $\omega = 17$ meV ($\lambda_i = 1.6$ Å, left) and $\omega = 7.5$ meV ($\lambda_i = 2.2$ Å, right) in AgCrS$_2$ at 2 and 70 K.

constant $\omega = 0.5$ meV in contrast with the Q scan at $\omega = 1.0$ meV [Fig. 4(c)].

At all temperatures, independent of the magnetic ordering, a signal extending over a broad-Q range, and whose intensity increases with increasing Q, is observed around $\omega = 3$ meV; decreasing the temperature leads to a significant decrease in the intensity of this signal on the $S(Q,\omega)$ maps, suggesting a phonon-like excitation. This low-frequency phonon has been studied in detail in the 10–800-K temperature range[22] and has been identified as a transverse optical phonon resulting from a strongly anisotropic in-plane motion of the Ag$^+$ ions, down to low temperatures. Within the experimental resolution, there is no change in the energy of this phonon at T_N.

B. Classical energy calculations

To narrow down the number of parameters involved in the spin-wave modeling of the inelastic-scattering results, the magnetic phase diagram of a distorted triangular lattice has been investigated as a function of the different relevant
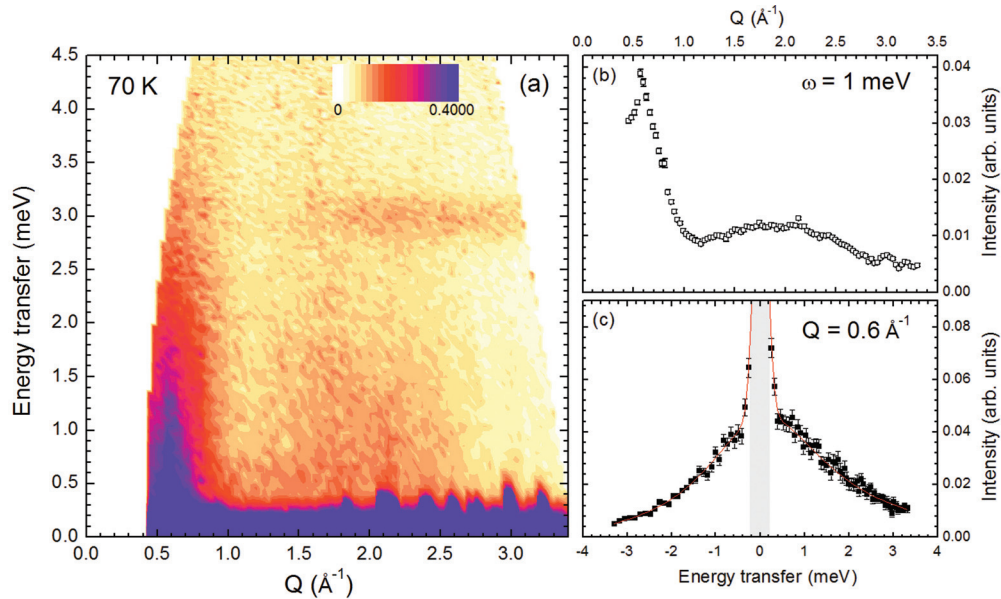
FIG. 3. (Color online) $S(Q,\omega)$ map (IN4 data, $\lambda = 3.2$ Å) of polycrystalline AgCrS$_2$ at (a) 70 K, (b) corresponding profiles at constant energy transfer $\omega = 1$ meV, and (c) constant momentum transfer $Q = 0.6$ Å^{-1}. The gray area shows the incoherent elastic signal, modeled using a Gaussian with a FWHM equal to the instrumental resolution.

magnetic interactions illustrated in Figs. 1(b) and 1(c). The distortion of the triangular lattice is taken into account using a simple monoclinic cell (identified with the subscript m) with $a_m = (a_R - b_R)$, $b_m = a_R + b_R$, and $c_m = (c_R - a_R + b_R)/3$ with respect to the original rhombohedral structure (identified with the subscript R) corresponding to perfect triangular layers stacked in a $ABCABC\ldots$ fashion. There are two

nonsymmetry-related Cr^{3+} sites in the magnetic cell. The two nearest-neighbor interactions are labeled J_{ab} and J'_{ab} and correspond, respectively, to the exchange paths alongside the long Cr-Cr distances parallel to $[010]_m$ and to the shorter Cr-Cr distances along $[\frac{1}{2} \frac{1}{2} 1]_m$ and $[\frac{1}{2} -\frac{1}{2} 1]_m$ [see Fig. 1(b), according to Ref. 17]. Similarly, there are two next-nearest-neighbor interactions J_{NN} and J'_{NN} (the monoclinic distortion
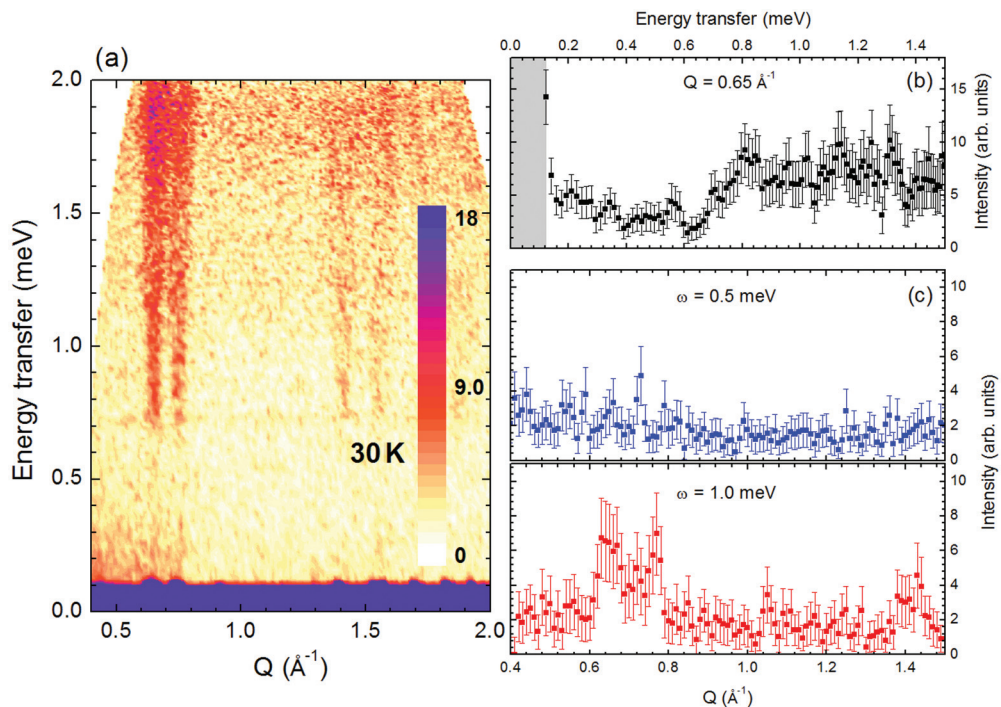
FIG. 4. (Color online) $S(Q,\omega)$ maps of polycrystalline AgCrS$_2$ at (a) 30 K (IN5 data, $\lambda_i = 5.0$ Å), (b) corresponding profiles at constant momentum transfer $Q = 0.65$ Å^{-1}, and (c) constant energy transfer $\omega = 0.5$ and 1 meV.
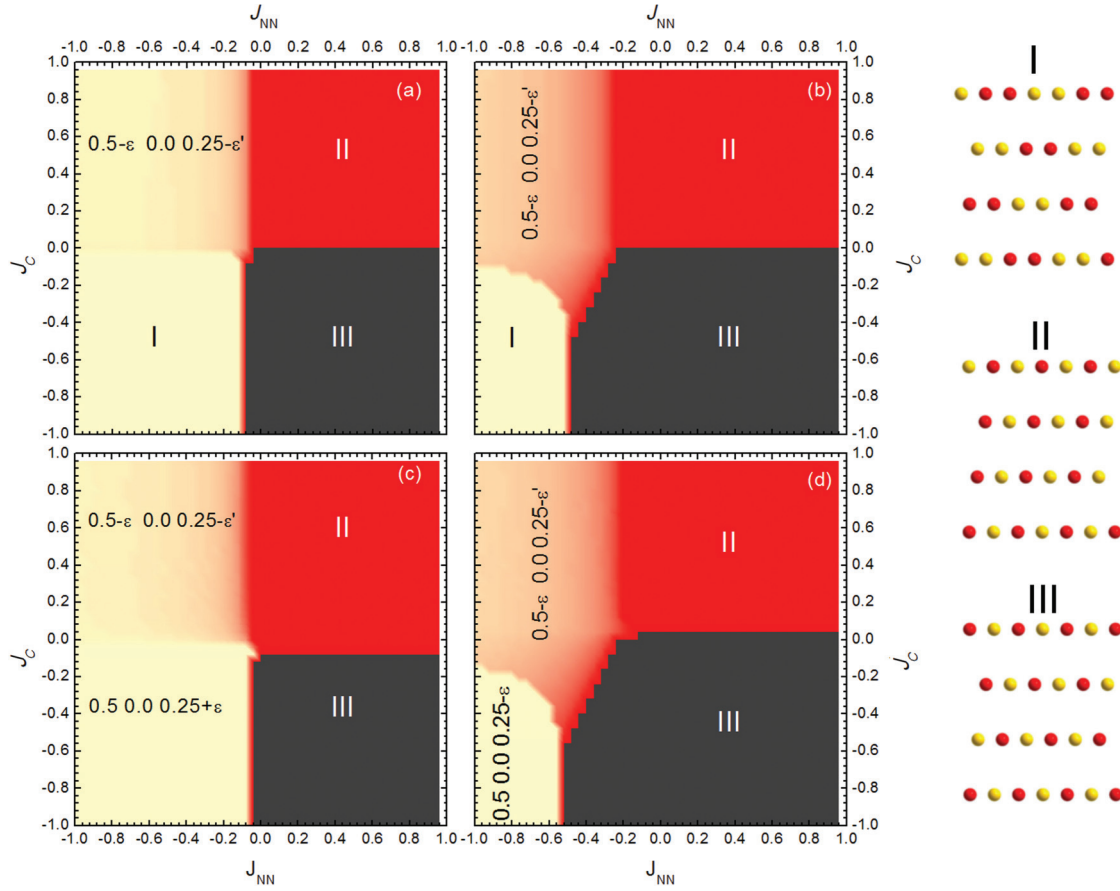
FIG. 5. (Color online) Magnetic phase diagrams showing the dependence of the magnetic propagation vector **k** as a function of (J_{NN}, J_C) for a normalized $J_{ab} = 1$ with (a) $J'_{ab} = -0.1$ and $J'_{NN} = J'_C = 0$, (b) $J'_{ab} = -0.5$ and $J'_{NN} = J'_C = 0$, (c) $J'_{ab} = -0.1$, $J'_{NN} = 0$, and $J'_C = -0.1$, and (d) $J'_{ab} = -0.5$, $J'_{NN} = 0$, and $J'_C = 0.1$. The definition of the different J's is given in Figs. 1(b) and 1(c). On the right side are illustrated the projections along $[010]_m$ of the three commensurate magnetic phases, labeled I, II, and III, appearing in the phase diagram and which correspond to the propagation vectors (0.5 0 0.25), (0 0 0), and (0 0 0.5), respectively.

leads to a shorter Cr-Cr distance along the $[102]_m$ direction corresponding to the J_{NN} path) and two interplane couplings J_C and J'_C as the distortion also lifts the degeneracy of the two interlayer exchange paths [Fig. 1(c)]. All the above interactions are supposed to be Heisenberg-like. The magnetic Hamiltonian of AgCrS$_2$ can, thus, be expressed as

$$\mathcal{H} = \mathcal{H}_{ab} + \mathcal{H}_{NN} + \mathcal{H}_C, \qquad (1)$$

with

$$\mathcal{H} = \sum_{i,j} J_{ij} S_i S_j + D_n \sum_i (S_i n)^2. \qquad (2)$$

It takes into account exchange couplings acting between neighboring spins as well as single-ion anisotropy D. If D is negative, it accounts for an easy-axis anisotropy with n being the easy-axis direction. In the mean-field approximation, it can be used to explore the stable magnetic structures, defined by their propagation vector **k** as a function of the exchange interactions described above. Note that the (0 0 0.25) magnetic structure described in the complex Cm monoclinic cell of AgCrS$_2$ (Ref. 17) corresponds, in the setting chosen here, to a propagation vector of the type $\mathbf{k}_{4SL} = (0.5\ 0\ 0.25)$. In preliminary investigations of the magnetic phase diagram of AgCrS$_2$, it was found that introducing an antiferromagnetic J_{ab} exchange always leads to magnetic propagation vectors with an incommensurate component along b_m. Consequently, the J space was narrowed down to include only ferromagnetic J_{ab} in the calculations of the phase diagrams presented here with **k** vectors of the form $(k_x, 0, k_z)$. This result is further supported by the fact that, in the distorted lattice, the J_{ab} exchange path is along the longest Cr-Cr distance ($\sim$3.50 Å), close to the threshold value of 3.6 Å determined by Engelsman *et al.*[20] and Rosenberg *et al.*[23] in their study of various chromium sulfides and selenides to give rise to a ferromagnetic exchange interaction. The fact that ferromagnetic exchange paths are found for large Cr-Cr distances has also recently been confirmed in an inelastic-scattering study of AgCrSe$_2$.[24]

Calculations also showed that the (0.5 0 0.25) magnetic phase characterizing AgCrS$_2$ cannot be stabilized for a

ferromagnetic J'_{ab}. The (J_{NN}, J_C) phase diagrams obtained for different values of J'_{ab} (<0) and J'_C are illustrated in Fig. 5. In Fig. 5(a), which corresponds to $J'_{ab}/J_{ab} = -0.1$, four magnetic phases can be distinguished: The 4SL phase is stable only for an antiferromagnetic J_C and an antiferromagnetic J_{NN} with $|J_{NN}| > |J'_{ab}|$. A larger J'_{ab} will result in a larger J_{NN} to stabilize the 4SL phase, whose existence range is, therefore, reduced [see Fig. 5(b)] to the benefit of a C-type-like phase (antiferromagnetic arrangement of ferromagnetic chains parallel to $[010]_m$) and an incommensurate one of the type $(0.5 - \varepsilon, 0, 0.25 - \varepsilon')$. As can be deduced from Fig. 1(b), introducing a J'_{NN} interaction in (1) has the same consequences on the phase diagram as modifying J'_{ab}, both effects adding up. In contrast, introducing a J'_C term, whether ferro- or antiferromagnetic, in the Hamiltonian, leads to the destabilization of the 4SL phase to the benefit of a related but incommensurate one in the c_m direction [Figs. 5(c) and 5(d)].

Using these simple mean-field calculations, it appears that the 4SL phase of AgCrS$_2$ can be stabilized taking into account a ferromagnetic J_{ab} and antiferromagnetic J_{NN} and J_C with $(J'_{ab} + J'_{NN})$ antiferromagnetic and $|J_{NN}| > |J'_{ab} + J'_{NN}|$ and with $D = 0$. Accordingly, the value of the next-nearest-neighbor coupling J_{NN} has to be large enough to overcome the destabilizing effect of J'_{ab} and underlines the major role of this interaction. In contrast to the perfect triangular lattice, in which it has been shown to induce incommensurability with respect to the 120° phase,[8] J_{NN} stabilizes a collinear magnetic phase in the case of an antiferromagnetic J_C. Adding an axial anisotropy term D in the model Hamiltonian—to reproduce the experimental evidence of a gap in the excitation spectrum—stabilizes the collinear phases with respect to the incommensurate ones, thus, modifying the phase diagrams of Fig. 5. In particular, it becomes possible to stabilize the 4SL phase with a nonzero J'_C; however, if this anisotropy term is kept small, the stability range of the 4SL phase is only slightly modified, and the conclusions drawn on the relative values of the different exchanges are still valid.

C. Spin-wave simulations

To model the spin dynamics, spin-wave calculations were performed using the SPINWAVE software developed at Laboratoire Léon Brillouin. Based on the Holstein-Primakov approximation, the code diagonalizes the chosen spin Hamiltonian; in the present case, the calculations were performed using isotropic exchange couplings and an easy-axis anisotropy term along $[010]_m$. $S(Q, \omega)$ is first calculated over a sphere in the reciprocal space, and powder averaging is performed sampling the sphere following a Fibonacci-based algorithm.[25] The validity of this type of calculations was first tested by comparing the powder averaged $S(Q, \omega)$ calculated from a set of J's taken from a recent CuCrO$_2$ single-crystal neutron-inelastic-scattering study[8] with the experimental data of polycrystalline CuCrO$_2$ at 5 K.[26] According to the mean-field results presented in the previous section, the following magnetic exchange parameters were introduced in (1): J_{ab}, J'_{ab}, J_{NN}, J_C, and $D_{[010]_m}$ ($D < 0$) to keep the modeling as simple as possible. The value of J'_{ab} does not have a major impact on the excitation spectrum and was chosen weakly antiferromagnetic to keep the range of (J_{NN}, J_C) in which the

4SL phase is stable as large as possible. Aside from the $D_{[010]_m}$ term, which is easily determined, there are two features of the excitation spectrum which are visible on the $S(Q, \omega)$ maps and three parameters to find so that several sets of exchange parameters leading to a reasonable agreement between the simulated scattering map and the data can be obtained. However, calculations show rather clearly that the energy position of the ~ 8 meV feature is mainly controlled by $J_{NN} + \alpha J_C$ ($\alpha > 1$), whereas, the energy position of the top of the band depends roughly on the sum of all exchange interactions: As a result, if J'_{ab} is kept negligible, J_{ab} can be estimated rather precisely, whereas, uncertainty remains concerning the ratio between J_{NN} and J_C. Figure 6(a) illustrates an example of the dynamical structure factor calculated for the set of parameters $J_{ab} = 1.80$, $J'_{ab} = -0.05$, $J_{NN} = -1.00$, $J_C = -0.60$, and $D_{[010]_m} = -0.03$ meV, which leads to a satisfactory agreement with the experimental data [Fig. 6(b)]. It is to be compared with Fig. 6(c), which shows the excitation spectrum of AgCrS$_2$ calculated with the following parameters: $J_{ab} = 1.70$, $J'_{ab} = -0.15$, $J_{NN} = -0.80$, $J_C = -0.80$, and $D_{[010]_m} = -0.03$ meV and which also reasonably reproduces the experimental spectrum. Assuming J'_{ab} remains weak, according to the stability domain calculated in the phase diagram, J_{ab} can, therefore, be estimated to be 1.8(2) meV. As mentioned above, J_{NN} and J_C parameters are strongly correlated in the powder averaging of the excitation spectrum; the best qualitative results, nevertheless, are obtained for $J_{NN} + J_C \sim 1.6(2)$ meV with J_{NN} and J_C values in the range of 0.4–1.2 meV. In particular, for $J_C \gg J_{NN}$ and outside the specified range—a fairly unlikely hypothesis given the distance between magnetic layers—magnetic scattering is calculated below the 8-meV feature.

As shown in Fig. 7 in the case of $J_{ab} = 1.80$, $J'_{ab} = -0.05$, $J_{NN} = -1.00$, $J_C = -0.60$, and $D_{[010]_m} = -0.03$ meV, the calculation also properly reproduces the fine details of the low-energy and low-momentum transfer part of the dispersion seen on the $\lambda_i = 5$-Å data [Fig. 7(c)], and in particular, the weak easy-axis-like anisotropy gap [Fig. 7(b)], further corroborating the validity of the model.

Based on this simple approach, both mean-field calculations and inelastic-neutron-scattering data, therefore, confirm that, in AgCrS$_2$, the 4SL phase is a consequence of a strong ferromagnetic coupling along the stripes with substantial antiferromagnetic J_{NN} coupling perpendicularly to the stripes.

D. Discussion

The role of the lattice distortion—which is also observed in other sulfides, such as CuCrS$_2$ (Ref. 27) and AuCrS$_2$ (Ref. 28)—is significant in AgCrS$_2$: It leads, in particular, to a ferromagnetic coupling along one direction of the triangle, following the threshold scenario in which the J_{ab} exchange changes sign for a Cr-Cr distance above ~ 3.50 Å. Another unusual aspect of AgCrS$_2$ is the particularly large value of the next-nearest exchange J_{NN}: Based on the data modeling, it is on the order of ~ -1 meV, e.g., four times larger than in CuCrO$_2$,[8] despite the fact that the corresponding second-neighbor Cr-Cr distance is much larger in the sulfide than in the oxide (6.03 Å on average in AgCrS$_2$ against 5.14 Å in CuCrO$_2$). With such a large value of J_{NN}, it is arguable from classical energy
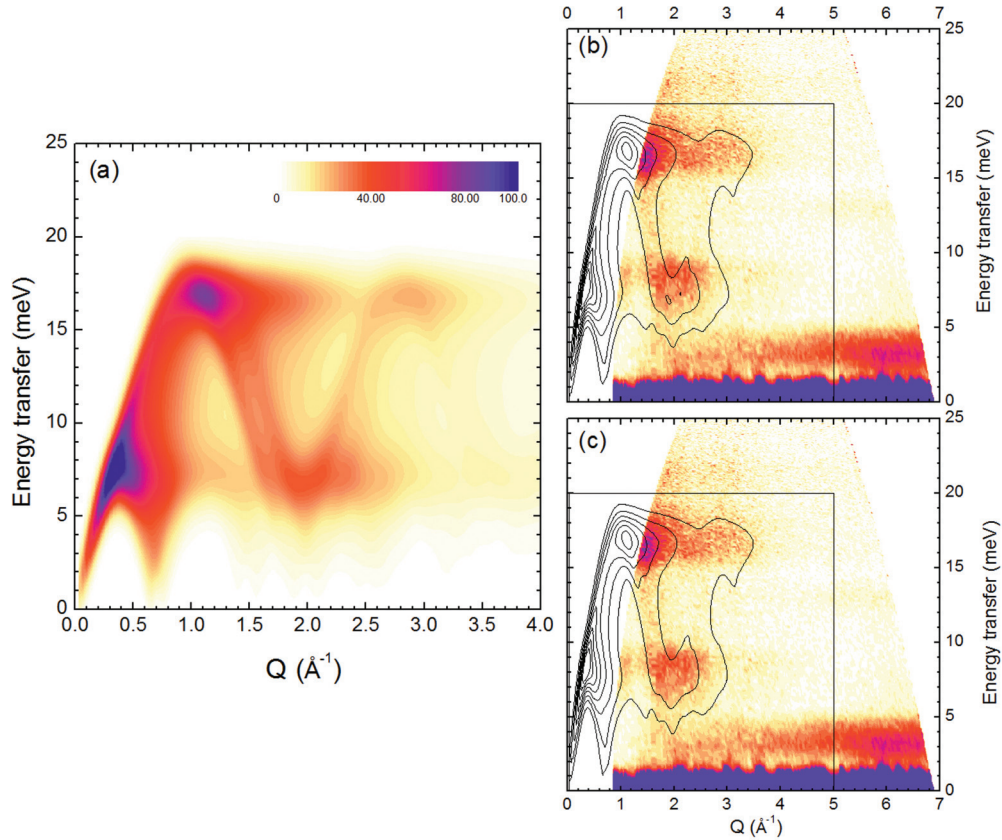
FIG. 6. (Color online) (a) Powder average calculation of the magnetic excitations spectrum of AgCrS$_2$, using $J_{ab} = 1.80$, $J'_{ab} = -0.05$, $J_{NN} = -1.00$, $J_C = -0.60$, and $D_{[010]_m} = -0.03$ meV, and the superposition with the experimental data at 2 K for $\lambda_i = 1.6$ Å is shown in (b). (c) The same as (b) for a calculation based on the following parameters: $J_{ab} = 1.70$, $J'_{ab} = -0.15$, $J_{NN} = -0.80$, $J_C = -0.80$, and $D_{[010]_m} = -0.03$ meV.

calculations[8] that the magnetic ground state within a triangular plane would be, without the distortion, not the 120° structure associated with the (1/3 1/3) propagation vector but, rather, the collinear C-type ordering associated with a propagation vector (1/2 1/2). In such a C-type magnetic ordering, there is actually a ferromagnetic ordering along the $[110]_R$ direction, which is reminiscent of the one observed in AgCrS$_2$ along b_m: In the latter, the 4SL structure becomes the new magnetic ground state as the distortion of the crystal structure lifts the sixfold degeneracy of the J_{NN} paths, lowering the classical energy if $J_{ab} > |J'_{ab}|$.

The quasielastic magnetic signal observed above T_N is actually related to the magnetic ground state before the distortion and is, therefore, instructive in this context. In materials where magnetic ordering is precluded by competing interactions, a large quasielastic scattering is often seen, which can be decomposed into an elastic and a quasielastic part, whose contributions increase and decrease, respectively, when temperature is lowered.[29] Accordingly, a detailed analysis of the Q width and of the energy range, along with the evolution vs temperature of the quasi-elastic-scattering signal of AgCrS$_2$ could provide useful information about the magnetic exchange topology above T_N, that is, before the symmetry lowering of the lattice.

In contrast with AgCrS$_2$, in other examples of layered oxides in which distortion releases the frustration of the triangular lattice, such as CuMnO$_2$ or CuFeO$_2$, the role of the Ising-like anisotropy is prominent. In CuMnO$_2$,[30] at the collinear magnetic-ordering temperature, the triangular lattice becomes scalene with three different Mn-Mn distances. Excitations are gapped,[31] and it is thought that the strong anisotropy of the Mn moment in its environment prevents the 120° ordering to establish, stabilizing a collinear arrangement, instead. This is akin to an Ising-like situation, and the only resource for the system to release the frustration of the antiferromagnetic exchange is the lattice distortion. In CuFeO$_2$, the system undergoes a lattice distortion at the onset of the 4SL magnetic ordering from a R$\bar{3}$m to a monoclinic $C2/m$ symmetry,[32] which only partially lifts the degeneracy of the exchange paths, such as in AgCrS$_2$. The 4SL magnetic ordering in CuFeO$_2$ is actually different from the one observed in AgCrS$_2$ as the spin arrangement along $[010]_m$ is not ferromagnetic but antiferromagnetic. Based on calculations performed on perfect triangular lattices, Ising-like anisotropy is needed to stabilize such a structure[33] in agreement with inelastic-neutron-scattering measurements evidencing an easy-axis gap of ~0.9 meV in the spin-wave excitations.[34] The impact of the spin-driven lattice distortion on the exchange interactions in
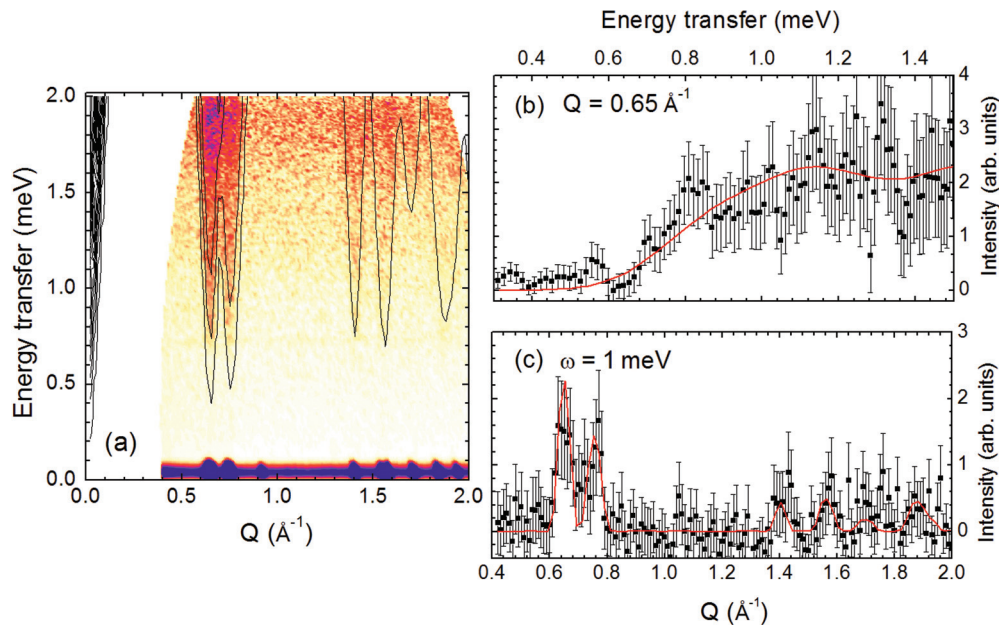
FIG. 7. (Color online) (a) Superposition of the calculation (using $J_{ab} = 1.80$, $J'_{ab} = -0.05$, $J_{NN} = -1.00$, $J_C = -0.60$, and $D_{[010]_m} = -0.03$ meV) with the experimental data at 30 K for $\lambda_i = 5.0$ Å. For a more quantitative comparison, (b) the corresponding intensity profiles at constant $Q = 0.65$ Å^{-1} and (c) constant $\omega = 1$ meV are also shown (black symbols: experimental data; red line: calculated profile). The experimental data have been corrected by the Bose factor.

$CuFeO_2$ was also investigated recently:[35] The magnitude, but not the sign, of the first-neighbor exchange is significantly modified by the distortion. The same observation applies to the second- and third-neighbor in-plane exchanges as well as interplane interactions, emphasizing the need to take into account the symmetry lowering of the exchange paths in the magnetic phase diagram calculations of this system.

Note here that, in the chromium delafossite $CuCrO_2$, no lattice distortion has been evidenced so far,[7] and the magnetic ground state is close to that expected for Heisenberg spins on a perfect triangular lattice.[8]

In sulfide systems, magnetoelastic effects are more often encountered than in their oxide counterparts as they are less ionic, and the electrostatic term in the global energy of the system is comparatively small.[36] A detailed comprehension of the effect of bond length on the magnetic exchange sign is necessary at this stage; nevertheless, a small electrostatic energy term, along with a strong spin-lattice coupling, are two key characteristics to take into account to understand ferroelectricity in $AgCrS_2$. Going further is challenging, however, as the magnetoelastic coupling and the fact that the crystal structure of $AgCrS_2$ should be polar above and below T_N make it difficult to determine the macroscopic mechanism behind ferroelectricity. Large atomic displacements, resulting from the shearing of the planes perpendicular to c_R, subsequent to the lattice distortion, could be invoked, that would lead to a polarization vector lying in the ac plane of the monoclinic cell.[17] A more-complex scenario, similar to the one proposed in Ref. 37 for the related 4SL magnetic structure of the $HoMnO_3$ perovskite, could involve transverse shifts in the sulfur atoms along the ↑↑↓↓ chains to modulate the Cr-S-Cr angle depending on whether adjacent spins are parallel or antiparallel [note that this can also affect the magnitude of the exchange interaction as in the model proposed for $CuFeO_2$ (Ref. 35)]. This should lead to a polarization vector lying along b_m. These mechanisms remain to be evidenced yet in $AgCrS_2$ as they are beyond the experimental resolution of powder scattering.

IV. CONCLUSION

Inelastic-scattering experiments combined with mean-field and spin-wave calculations have shown that the unusual four-sublattice magnetic ground state of $AgCrS_2$ can be stabilized considering a ferromagnetic first-neighbor exchange along the longest Cr-Cr distance of the monoclinic cell and a large antiferromagnetic second-neighbor exchange J_{NN} perpendicular to these ferromagnetic chains. The exchange along the two shortest Cr-Cr distances of the distorted cell remains weakly antiferromagnetic. This shows that, by changing the sign of the first-neighbor interaction, the lattice degree of freedom is the key to the stabilization of the collinear 4SL magnetic structure of $AgCrS_2$.

*francoise.damay@cea.fr

[1] M. Fiebig, J. Phys. D: Appl. Phys. **38**, R123 (2005).

[2] R. Ramesh and N. A. Spaldin, Nat. Mater. **6**, 21 (2007).

[3] T. Kimura, T. Goto, H. Shintani, K. Ishizaka, T. Arima, and Y. Tokura, Nature (London) **426**, 55 (2003).

[4] N. Hur, S. Park, P. A. Sharma, J. S. Ahn, S. Guha, and S. W. Cheong, Nature (London) **429**, 392 (2004).

[5] T. Kimura, J. C. Lashley, and A. P. Ramirez, Phys. Rev. B **73**, 220401 (2006).

[6] N. Terada, T. Nakajima, S. Mitsuda, H. Kitazawa, K. Kaneko, and N. Metoki, Phys. Rev. B **78**, 014101 (2008).

[7] M. Poienar, F. Damay, C. Martin, V. Hardy, A. Maignan, and G. André, Phys. Rev. B **79**, 014412 (2009).

[8] M. Poienar, F. Damay, C. Martin, J. Robert, and S. Petit, Phys. Rev. B **81**, 104411 (2010).

[9] S. Seki, Y. Onose, and Y. Tokura, Phys. Rev. Lett. **101**, 067204 (2008).

[10] J. L. Soubeyroux, D. Fruchart, C. Delmas, and G. Leflem, J. Magn. Magn. Mater. **14**, 159 (1979).

[11] C. Delmas, G. Leflem, C. Fouassier, and P. Hagenmuller, J. Phys. Chem. Solids **39**, 55 (1978).

[12] Y. Oohara, S. Mitsuda, H. Yoshizawa, N. Yaguchi, H. Kuriyama, T. Asano, and M. Mekata, J. Phys. Soc. Jpn. **63**, 847 (1994).

[13] S. Mitsuda, N. Kasahara, T. Uno, and M. Mase, J. Phys. Soc. Jpn. **67**, 4026 (1998).

[14] H. Katsura, N. Nagaosa, and A. V. Balatsky, Phys. Rev. Lett. **95**, 057205 (2005).

[15] T. H. Arima, J. Phys. Soc. Jpn. **76**, 073702 (2007).

[16] K. Singh, A. Maignan, C. Martin, and C. Simon, Chem. Mater. **21**, 5007 (2009).

[17] F. Damay, C. Martin, V. Hardy, G. Andre, S. Petit, and A. Maignan, Phys. Rev. B **83**, 184413 (2011).

[18] H. Hahn and C. De Lorent, Z. Anorg. Allg. Chem. **290**, 68 (1957).

[19] P. F. Bongers, C. VanBrugg, J. Koopstra, W. P. F. Omloo, G. A. Wiegers, and F. Jellinek, J. Phys. Chem. Solids **29**, 977 (1968).

[20] F. Engelsman, G. A. Wiegers, F. Jellinek, and B. VanLaar, J. Solid State Chem. **6**, 574 (1973).

[21] F. Wang and A. Vishwanath, Phys. Rev. Lett. **100**, 077201 (2008).

[22] P. Brüesch, T. Hibma, and W. Bührer, Phys. Rev. B **27**, 5052 (1983).

[23] M. Rosenberg, A. Knülle, H. Sabrowsky, and C. Platte, J. Phys. Chem. Solids **43**, 87 (1982).

[24] M. Brandlein, F. Damay, S. Petit, G. Andre, C. Martin, and A. Maignan (unpublished).

[25] J. H. Hannay and J. F. Nye, J. Phys. A **37**, 11591 (2004).

[26] S. Petit (unpublished).

[27] J. C. E. Rasch, M. Boehm, C. Ritter, H. Mutka, J. Schefer, L. Keller, G. M. Abramova, A. Cervellino, and J. F. Loffler, Phys. Rev. B **80**, 104431 (2009).

[28] S. J. E. Carlsson, G. Rousse, I. Yamada, H. Kuriki, R. Takahashi, F. Levy-Bertrand, G. Giriat, and A. Gauzzi, Phys. Rev. B **84**, 094455 (2011).

[29] J. A. Mydosh, *Spin Glasses: An Experimental Introduction* (Taylor & Francis, London/Washington, D.C., 1993).

[30] F. Damay, M. Poienar, C. Martin, A. Maignan, J. Rodriguez-Carvajal, G. Andre, and J. P. Doumerc, Phys. Rev. B **80**, 094410 (2009).

[31] C. Stock (private communication).

[32] F. Ye, Y. Ren, Q. Huang, J. A. Fernandez-Baca, P. C. Dai, J. W. Lynn, and T. Kimura, Phys. Rev. B **73**, 220404 (2006).

[33] R. S. Fishman, G. Brown, and J. T. Haraldsen, Phys. Rev. B **85**, 020405 (2012).

[34] F. Ye, J. A. Fernandez-Baca, R. S. Fishman, Y. Ren, H. J. Kang, Y. Qiu, and T. Kimura, Phys. Rev. Lett. **99**, 157201 (2007).

[35] T. Nakajima, A. Suno, S. Mitsuda, N. Terada, S. Kimura, K. Kaneko, and H. Yamauchi, Phys. Rev. B **84**, 184401 (2011).

[36] D. Vaughan and M. Rosso, Rev. Mineral. Geochem. **61**, 231 (2006).

[37] J. van den Brink and D. I. Khomskii, J. Phys.: Condens. Matter **20**, 434217 (2008).